Astron. Astrophys. 358, 1058–1068 (2000)

ASTRONOMY AND ASTROPHYSICS

# Expansion velocities and dynamical ages of planetary nebulae⋆

**K. Gesicki**[1] **and A.A. Zijlstra**[2]

[1] Centrum Astronomii UMK, ul. Gagarina 11, 87-100 Torun, Poland (gesicki@astri.uni.torun.pl)
[2] Astrophysics Group, Physics Department, UMIST, P.O. Box 88, Manchester M60 1QD, UK (aaz@iapetus.phy.umist.ac.uk)

Received 24 February 2000 / Accepted 16 April 2000

**Abstract.** The [O III] expansion velocities are presented for planetary nebulae in the Galactic Bulge and Halo, and in the Sagittarius Dwarf spheroidal galaxy. The velocities are shown to increase with the distance from the star, in agreement with hydrodynamical models. Dynamical ages are derived from these velocities and are corrected for the effects of post-AGB acceleration and non-uniform velocities. Masses for the central stars are obtained from relations between dynamical ages and stellar temperatures. The stellar core mass distribution is narrow, peaking at 0.61 $M_{\odot}$. This is higher than predicted for the Bulge by initial-final mass relations, but consistent with the local white dwarf mass distribution.

**Key words:** ISM: planetary nebulae: general – stars: white dwarfs

## 1. Introduction

The expansion velocity of a planetary nebula (PN) is the single most important parameter determining its evolution. Surprisingly, it is only known for about 300 PNe, mostly bright objects in the Galactic disk. The nebular expansion after the PN ejection occurs in conjunction with the increase in stellar temperature. While the nebular radius and its expansion velocity define the nebular dynamical age, the position of the central star in the HR diagram defines a post-mass-loss stellar age. If correctly determined, both ages should be equal. However, the two time scales correlate very poorly: the dynamical ages are on average much shorter than the stellar ages (e.g. Pottasch 1984 p.234). Possible reasons are that the distances are poorly known, leaving both the radius and luminosity uncertain, and that the expansion velocity may vary both with position in the nebula and with time.

Expansion velocities are known to vary. The [N II] expansion velocity is almost always larger than that in [O III] (Wilson 1950), indicating internal velocity fields for which a single velocity may be a poor representation (Gesicki et al. 1996, 1998; resp. paper I and II). Marten & Schönberner (1991), and recently Schönberner & Steffen (1999, 2000) present hydrodynamical calculations for an evolving PN. Their models always show velocity increasing with radius. This acceleration must be taken into account when deriving dynamical ages.

In this paper we will present the first expansion velocities for PNe in the Bulge, for which the distance is approximately known. Photo-ionization models are used to derive internal velocity fields, showing how the expansion velocity varies with radius. We calculate the original pre-PN outflow velocity, to estimate the effects of the acceleration over time. In this way, more robust dynamical ages can be derived.

Stellar time scales are very sensitive to the core mass (and therefore luminosity) of the star, with lower-mass stars evolving much slower. Even for objects at reasonably known distance, the PN luminosity cannot be determined to the required accuracy. The white dwarf mass distribution is quite narrow (e.g. Weidemann 1987), and as a result the full range of stellar luminosities is only about a factor of two. The uncertainties are of the same order, because of the need to convert from a nebular emission line flux to a stellar radiation field. We will show that the problem can be inverted: by requiring the new dynamical ages and stellar ages to be the same, the position in the HR diagram can be derived without using the uncertain luminosity. This will allow us to determine core masses for the central stars. Recently the masses of central stars of PNe were discussed by Gorny et al. (1997) and Stasinska et al. (1997) and we will compare their results with ours.

## 2. [O III] observations and sample selection

### *2.1. Bulge, disk and halo membership*

We present [O III] observations of 44 PNe, located primarily in the direction of the Galactic Bulge. However, this region also includes foreground disk objects, objects belonging to the inner halo, and two background PNe belonging to the Sagittarius Dwarf Galaxy (Sgr). Criteria for Bulge membership are: (1) within 15 degrees of the Galactic Centre; (2) distance $6\,\mathrm{kpc} \leq R \leq 10\,\mathrm{kpc}$; (3) metallicity greater than 0.1 of Solar. (Stellar kinematics in the centre of the galaxy indicates that stars with metallicity less than 0.1 of Solar belong to the inner halo (Minniti 1996).)

Abundances for PNe in our sample are given by Dudziak et al. (2000) for the two objects in Sgr, and by Cuisinier et al.

*Send offprint requests to*: K. Gesicki

⋆ Based on observations obtained at ESO

(2000), Ratag et al. (1997), Costa et al. (1996), Webster (1988) and Aller & Keyes (1987) for most of the Galactic PNe. The Bulge membership criteria are satisfied by 26 objects. 14 objects appear to belong to the Galactic disk. The two Sgr objects Zijlstra & Walsh 1996) are He 2-436 (004.8–22.7) and Wray 16-423 (006.8–19.8).

Two objects are suggested to be halo PN: Hb8 because of its large indicated distance (see Sect. 3.1) and high latitude and M2-29 because of its very low metallicity.

### *2.2. Observations*

The observations were carried out with the ESO 1.4m CAT telescope in July 1993. The so-called short camera was used in the blue arm of the echelle spectrograph, with a resolution of 30000, corresponding to $6\,\mathrm{km\,s^{-1}}$. The [O III] $5007$ Å line was observed. Integration times varied from a few to 30 minutes depending on the line flux. Faint nebulae could not be observed because they were not visible on the finder due to the brightness of the Moon. The slit had a width of $2''$ and a length of $20''$. The pixel scale corresponded to $2''$. The wavelength calibration was done with ThAr spectra, and also checked by observing well-known planetary nebulae as velocity standards.

The data reduction involved flat fielding, cosmic-ray removal and wavelength calibration. The line profiles were summed over the slit to obtain an integrated spectrum, but for resolved nebulae the profile variation along the slit was also analyzed. Radial velocities determined from the spectra have been presented in Zijlstra et al. (1997).

## 3. Method of analysis

### *3.1. Computer codes*

For each nebula in the sample, a photo-ionization model was constructed to fit the published intensities of the emission lines. The nebula is approximated as a spherical shell defined by an inner and outer radius, a total mass, a radial density distribution and a radial velocity field. The central star is modelled using a black-body atmosphere. The free parameters of the photo ionization model are adjusted to obtain a good agreement between the observed and calculated H$\beta$ flux and the emission line ratios.

Subsequently, a radial velocity profile is assumed, with the velocity varying smoothly with radius. The predicted profile for the emission line is calculated by integrating the velocity field over the ionization equilibrium and resulting line emission coefficients. The slit parameters and seeing are used as input parameters for this calculation. Comparing the predicted profile with the observations allows one to correct the assumed velocity field. The photoionization model requires knowledge of stellar and nebular parameters as initial parameters. Distances and radii are mostly taken from Van de Steene & Zijlstra (1994), however other values are sometimes adopted. The effective stellar temperature and luminosity are taken from the literature, but are often slightly changed during the fit in order to reproduce the observed H$\beta$ flux and the line ratios (CGPN). The adopted nebular and stellar parameters are presented in Table 2. They are in succession: PN designation according to galactic coordinates, PN common name, central star's effective temperature and luminosity, assumed distance, outer radius, and the ionized mass.

The computer codes as well as the recipe for modelling the nebulae are described elsewhere. Below we list the most important limitations: for further details we refer to Paper I.

### *3.2. Model simplifications*

The model fits as performed in this paper allow more freedom than those in papers I and II, firstly because less is known for most objects from our sample, and secondly because only one spectral line was observed.

Most of the PNe in our sample have small angular diameters and high-resolution images are not available. Therefore the density distribution (especially the inner radius) cannot be determined from imaging data. For all objects, we used a density distribution in the shape of an inverted parabola, with the central density twice as large the density at the edge. This is closer to predictions from hydrodynamical models than a constant density (e.g. Marten & Schönberner 1991). The inner nebular radius is taken as 0.4 of the outer radius.

Because we only have data for the [O III] line which mainly probes the inner nebular region, the fitted velocity field was limited to a linearly increasing velocity. Whenever possible we assumed a constant velocity. There are some indications of a steeper velocity gradient in the outer regions (as shown by wings on the line profile), but these can not be accurately modelled without information from lines formed in the outer regions, e.g. [N II].

Our calculated spectral lines are affected by thermal and instrumental broadening. The thermal broadening is calculated from the electron temperature indicated by the photoionization calculations and is different for each PN. The instrumental broadening corresponds to the spectral resolution of the instrument and is adopted as 0.17 Å. Additional turbulent motions may be present in a few nebulae, especially in those with [WC]-type nuclei (see Gesicki & Acker 1996), but this can be proven only by comparing the line widths from different ions (especially hydrogen is desirable). We therefore neglect the effects of possible turbulence.

### *3.3. Uniform velocities*

The models relate the line profile to a 'true' expansion velocity. Previously, expansion velocities were determined directly from the line profiles. For the case of a constant velocity throughout the nebula, we can quantify the difference between the expansion velocity as obtained from the line profile, and the 'true' model velocity. (For a non-uniform velocity the relations are very complicated.)

The observed line profile will depend on whether the slit resolves the nebula, e.g. line splitting is only seen for a spherically symmetric nebula if the slit width is smaller than the object. The effect of the relative size of the aperture on the derived expansion

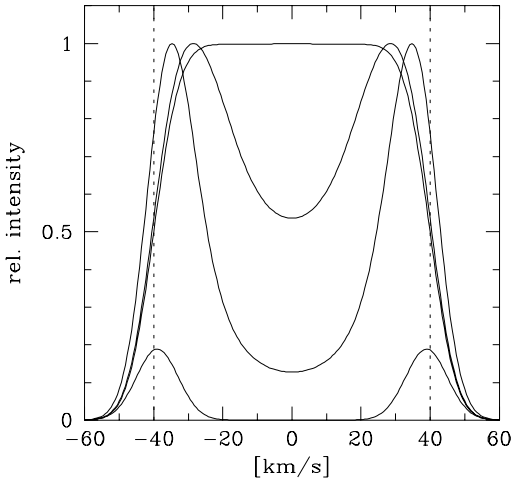


**Fig. 1.** Modelled [O III] lines for a spherical nebula with constant velocity and emissivity. This nebula is observed with a centered circular aperture: the profiles are given for aperture size relative to the PN diameter of: 1.0, 0.8, 0.5, 0.2. The vertical dashed line indicates the true expansion velocity of 40 km s$^{-1}$.

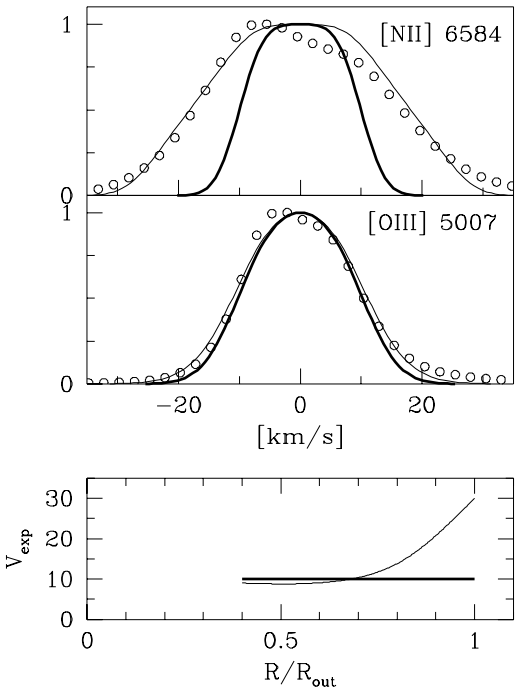


**Fig. 2.** [N II] 6584 Å and [O III] 5007 Å lines for object H 1-35 (PN G 355.7-03.5). The circles present the observed profiles, and the lines the modelled ones. Thick and thin lines correspond to two different velocity fields shown in the lowest box as a function of the relative nebular radius.

velocity is illustrated in Fig. 1, showing the calculated emission line profile for an artificial nebula with all parameters constant with radius. The line profiles in the figure correspond to circular apertures of different sizes. Table 1, lists, for different apertures, the ratio between the true expansion velocity, and the velocity derived from (*i*) line splitting, (*ii*) half width at half maximum (HWHM), (*iii*) half width at ten per cent of maximum (HWTP).

Most catalogued PNe expansion velocities are derived from the line splitting as $v_{\rm exp}$. This can significantly underestimate the true expansion velocity: the peak-to-peak separation is a good measure of the expansion velocity only if the nebula is fully resolved (e.g. Robinson et al. 1982). The half-width-at-half-maximum is the most accurate approximation to the true expansion velocity for spatially unresolved or marginally resolved nebulae. However, it overestimates the expansion velocity for well-resolved objects. Thirdly, the half-width at 10 percent of the peak (as used by Dopita et al. 1985) is almost independent of the size of the aperture but overestimates the true value by about 10 per cent. We note that the precise values depend on the relative effect of thermal broadening which increases for lower expansion velocities.

### *3.4. Velocity gradients*

Fig. 1 illustrates another important feature: the emission profile from a shell with uniform emissivity and constant expansion velocity is flat-topped when the nebula is unresolved. It would be rectangular in shape without line broadening (thermal, turbulent or instrumental): the flat top is visible when the expansion velocity is larger than the broadening. This can be seen as follows. When the spherical nebula expands with a constant velocity $v_{\rm exp}$ the Doppler-shifted contribution to the spectral line from a small volume element will depend on the angle ($\theta$) between the line connecting the nebular center with the element and the line

**Table 1.** The expansion velocities defined for the models shown in Fig. 1, determined from line splitting (e.g. Weinberger 1989), half width at half maximum (Robinson et al. 1982) and the half width at ten per cent (Dopita et al. 1985), divided by the true expansion velocity.

| aperture | $V_{\rm split}/V_{\rm exp}$ | $V_{\rm HWHM}/V_{\rm exp}$ | $V_{\rm HWTP}/V_{\rm exp}$ |
|---|---|---|---|
| 1 | – | 1.00 | 1.13 |
| 0.8 | 0.73 | 1.00 | 1.10 |
| 0.5 | 0.80 | 1.08 | 1.10 |
| 0.2 | 0.89 | 1.15 | 1.16 |

from the center to the distant observer. The total contribution to the profile at the given velocity is obtained by integrating all volume elements at the appropriate $\theta$. Apply a spherical coordinate system, centered on the nebula and with the main axis pointing towards the observer. In such a system the volume element is:

$$dV = r^2 \sin\theta dr d\theta d\phi$$

After performing the integration over $d\phi$ (around the main axis) and over $dr$ (from 0 to $R$):

$$dV = \frac{2\pi}{3} R^3 \sin\theta d\theta$$

Consider the uniformly spaced intervals in the velocity $dv$. Because

$$dv = v_{\rm exp} \sin\theta d\theta,$$

equal intervals $dv$ in velocity correspond to equal volumes $dV$. Therefore the fluxes emitted in each velocity interval are equal

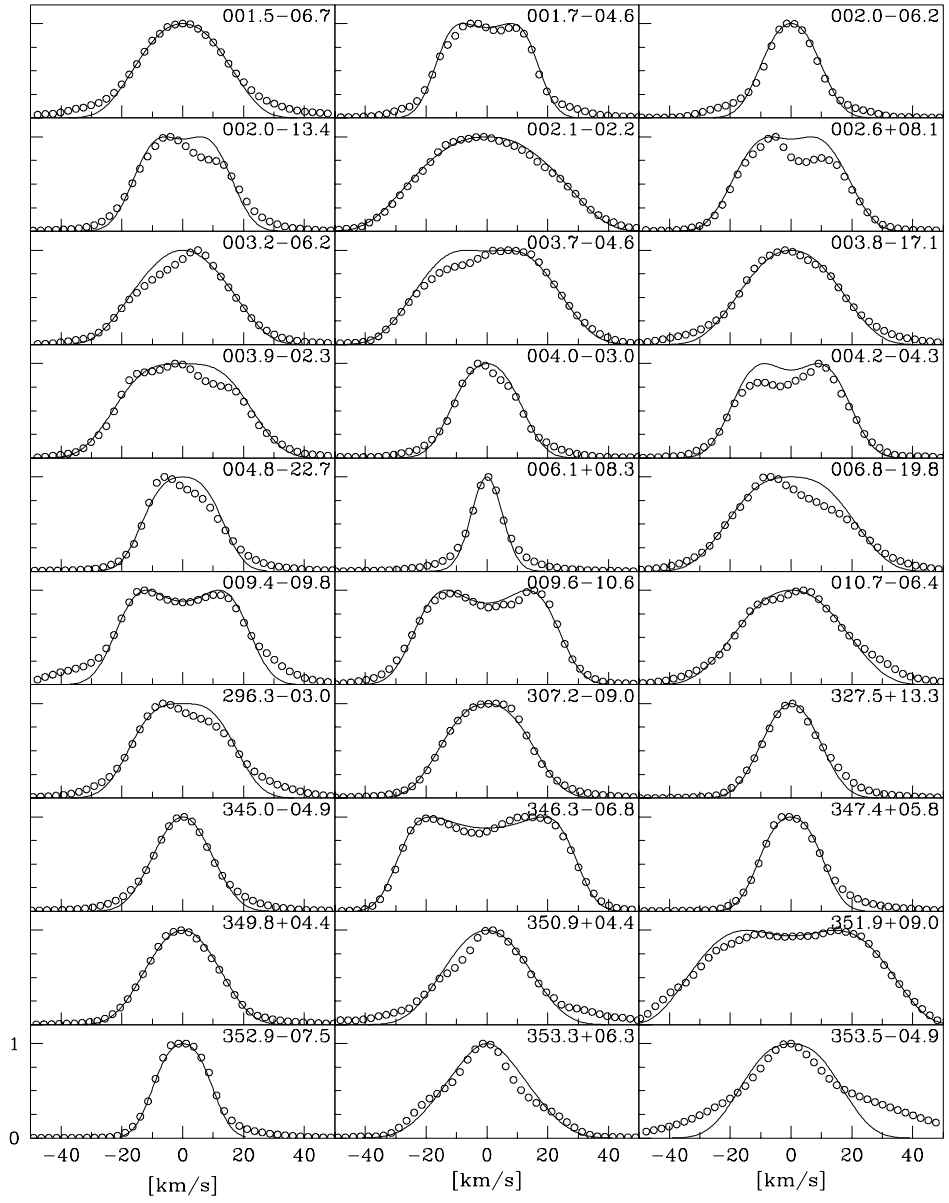


**Fig. 3.** Observed and modelled [O III] lines. The circles correspond to the observed profile, the lines to the fitted model. The ordinate of the plots is the relative intensity normalized to unity. The X and Y-axis scale given in the lowest boxes relates to all boxes.

and the spectral line is rectangular in shape. Such flat-topped lines are not observed, indicating that the velocity in our objects is more complicated. This is clear even from only one [O III] line formed near the nebular center.

The velocity fields presented in papers I and II, based on two or three lines, mostly show two components with a slowly increasing velocity in the inner nebula but steeply increasing in the outer parts. In Fig. 2 we present an example of this. For the nebula H 1-35 spectral lines of both [N II] 6584 Å (Acker, priv. comm.) and [O III] 5007 Å are shown. The bold line indicates a fit using only the [O III] line assuming a linear velocity field (this case is exceptional in that a constant velocity gives a reasonable fit). This fit fails for [N II]: instead the thin line shows a velocity profile which fits both lines. The nitrogen line shows evidence for a fast acceleration in the outer nebula. If only the [O III] line is available, the inner region of the nebula is well determined but the outermost velocities may be poorly constrained. This limitation should be kept in mind for the remainder of the paper.

## 4. Expansion velocities

### *4.1. Results*

The velocity fields resulting from fitting the [O III] lines are given in Table 2. We represent the velocity field of the model by two numbers: $\langle v_{\rm exp} \rangle$ is the mass-weighted average velocity and $\Delta v$ is the difference between the velocities at the outer and inner radius.

The expansion velocity $\langle v_{\rm exp} \rangle$ is defined in the same way as in Paper II, i.e. it is a mean value of the velocity field weighted by the mass distribution. This definition gives an average velocity which is more representative for the full nebula than using an unweighted value which would be more biased to the inner

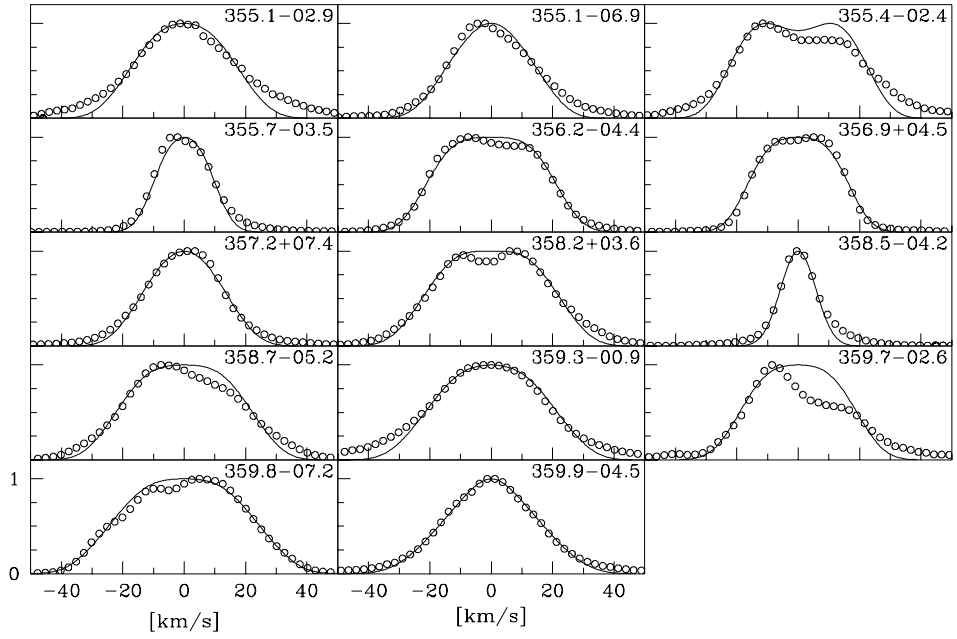


**Fig. 4.** Observed and modelled [O III] lines – continuation of Fig. 3

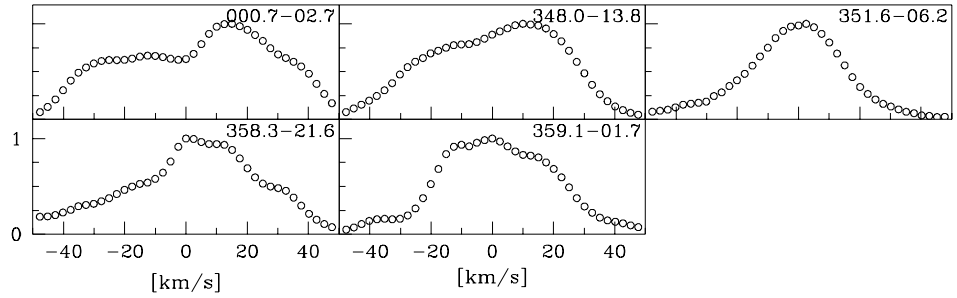


**Fig. 5.** Observed asymmetric [O III] lines. The presentation is the same as in Fig. 3.

region. A separate column lists the expansion velocity $v_{\rm HWHM}$ as estimated from the observed profiles. For PNe with a [WC]-type nucleus we can expect strong turbulent motions which are beyond present analysis; these objects are marked in the last column.

Almost all nebulae show indications of the presence of a velocity gradient. The few objects with constant expansion velocity ($\Delta v = 0$) show small expansion when broadening dominates. (One exception is PN G 001.7-04.6 with $\langle v_{\rm exp} \rangle = 17\,{\rm km\,s^{-1}}$ but in this case we model only the line core.) For two objects $< v_{\rm exp} >$ is very small and may not be representative for the full nebula. We are probably missing some kinematical component not visible in [O III] lines.

The observed lines with the calculated profiles superposed are presented in Fig. 3 and Fig. 4. Many observed profiles show extended wings indicating high velocity outflows not modelled by us. We believe that this corresponds to the situation discussed earlier and shown in Fig. 2. For M 3-32 (009.4-09.8), the long-slit spectrum reveals a bipolar nature, which is confirmed by the radio image (Zijlstra et al. 1989). The effect is not very pronounced and we kept this PN in our sample, but the spherically symmetric model should be treated with caution.

Almost all models are ionization bounded. If the line ratios could be adequately reproduced with an ionization-bounded model, this model was accepted. Only if no good fit could be obtained did we attempt to fit density-bounded models. In our sample only PC 13 (351.9+09.0), appears density bounded since otherwise its very weak [N II] 6584 Å line cannot be reproduced.

Table 3 and Fig. 5 present the velocities and line profiles for several PNe which were observed but for which the line profiles are too asymmetric for modelling. (In the case of 351.6-06.2, the velocities show a large gradient along the slit indicating a bipolar outflow. The spectrum shown in Fig. 5 appears symmetric only because it is summed over the slit.) These objects are not included in Fig. 6 since the values may not be a good representation for strongly aspherical nebulae. The non-symmetric, possibly bipolar objects show on average larger outflow velocities than the objects in Table 2.

Fig. 6 presents the histogram of the expansion velocities, in bins of $5\,{\rm km\,s^{-1}}$. Separately shown are the mass-weighted average velocities from the models (continuous line) and the HWHM values (dashed line). The model velocities peak between 20 and 30 $\rm km\,s^{-1}$ but the distribution shows a long wing towards smaller velocities. The HWHM velocities have a maximum at smaller values of about 15–20 $\rm km\,s^{-1}$. This difference can be easily understood, because the [O III] emission comes from layers where O III is the dominant ionization stage and the photoionization calculations show that this is always the

**Table 2.** The expansion velocities and derived data concerning the nebulae and the central stars. Remarks: 'wels' indicates a weak emission line star. Two nebulae are situated in the Sagittarius Dwarf galaxy and two objects may be halo PN.

| PN G | name | $\log T_{\rm eff}$ [K] | $\log(L)$ [$L_\odot$] | dist. [kpc] | $R_{\rm out}$ [pc] | $M_{\rm ion}$ [$M_\odot$] | $\langle v_{\rm exp}\rangle$ [km s$^{-1}$] | $\Delta v$ [km s$^{-1}$] | $v_{\rm HWHM}$ [km s$^{-1}$] | O/H | remarks |
|---|---|---|---|---|---|---|---|---|---|---|---|
| 001.5-06.7 | SwSt 1 | 4.58 | 4.10 | 4.0 | 0.02 | 0.05 | 28 | 37 | 17 | | [WC10] |
| 001.7-04.6 | H 1-56 | 4.95 | 3.00 | 10.0 | 0.08 | 0.12 | 17 | 0 | 17 | 8.73 | |
| 002.0-06.2 | M 2-33 | 4.74 | 3.30 | 8.0 | 0.10 | 0.27 | 12 | 14 | 10 | 8.69 | |
| 002.0-13.4 | IC 4776 | 4.60 | 3.60 | 3.5 | 0.06 | 0.18 | 22 | 26 | 17 | | wels |
| 002.1-02.2 | M 3-20 | 4.88 | 3.20 | 7.0 | 0.10 | 0.27 | 32 | 45 | 26 | 8.64 | |
| 002.6+08.1 | H 1-11 | 4.90 | 3.10 | 7.0 | 0.12 | 0.32 | 22 | 26 | 19 | 8.77 | |
| 003.2-06.2 | M 2-36 | 4.90 | 3.30 | 6.4 | 0.11 | 0.38 | 22 | 33 | 17 | 8.89 | |
| 003.7-04.6 | M 2-30 | 5.04 | 3.50 | 7.0 | 0.10 | 0.36 | 26 | 35 | 25 | 8.74 | |
| 003.8-17.1 | Hb 8 | 4.88 | 3.40 | 15.0 | 0.04 | 0.09 | 22 | 30 | 18 | | Halo PN? |
| 003.9-02.3 | M 1-35 | 4.90 | 3.60 | 4.5 | 0.05 | 0.17 | 26 | 26 | 23 | 8.48 | |
| 004.0-03.0 | M 2-29 | 4.88 | 3.30 | 9.0 | 0.08 | 0.23 | 14 | 15 | 12 | 7.46 | Halo PN? |
| 004.2-04.3 | H 1-60 | 4.90 | 3.00 | 7.0 | 0.10 | 0.21 | 21 | 22 | 20 | | [WC]? |
| 004.8-22.7 | He 2-436 | 4.95 | 3.70 | 25.0 | 0.03 | 0.09 | 14 | 10 | 13 | 8.36 | Sgr, [WC3] |
| 006.1+08.3 | M 1-20 | 4.90 | 3.40 | 6.0 | 0.04 | 0.09 | 2 | 0 | 6 | 8.62 | |
| 006.8-19.8 | Wray 16-423 | 5.00 | 3.60 | 25.0 | 0.05 | 0.18 | 26 | 32 | 21 | 8.33 | Sgr, wels |
| 009.4-09.8 | M 3-32 | 4.95 | 3.20 | 7.0 | 0.10 | 0.26 | 23 | 18 | 23 | | |
| 009.6-10.6 | M 3-33 | 4.95 | 3.30 | 8.0 | 0.12 | 0.40 | 25 | 20 | 25 | 8.45 | |
| 010.7-06.4 | IC 4732 | 4.82 | 3.60 | 8.0 | 0.08 | 0.29 | 25 | 33 | 20 | 8.42 | |
| 296.3-03.0 | He 2-73 | 5.00 | 3.70 | 4.0 | 0.04 | 0.11 | 19 | 21 | 18 | | |
| 307.2-09.0 | He 2-97 | 4.81 | 3.30 | 4.5 | 0.03 | 0.05 | 19 | 23 | 16 | | |
| 327.5+13.3 | He 2-118 | 4.90 | 3.00 | 7.0 | 0.03 | 0.03 | 13 | 18 | 11 | | |
| 345.0-04.9 | Cn 1-3 | 4.65 | 3.60 | 7.5 | 0.05 | 0.12 | 16 | 23 | 11 | | |
| 346.3-06.8 | Fg 2 | 5.08 | 3.20 | 8.7 | 0.10 | 0.22 | 30 | 10 | 30 | | |
| 347.4+05.8 | H 1-2 | 5.06 | 3.96 | 7.0 | 0.03 | 0.10 | 11 | 8 | 11 | | |
| 349.8+04.4 | M 2-4 | 4.74 | 3.80 | 6.0 | 0.05 | 0.16 | 17 | 23 | 13 | 8.80 | |
| 350.9+04.4 | H 2-1 | 4.52 | 3.87 | 5.0 | 0.03 | 0.06 | 36 | 50 | 15 | | |
| 351.9+09.0 | PC 13 | 4.95 | 3.90 | 6.0 | 0.10 | 0.15 | 29 | 42 | 34 | | |
| 352.9-07.5 | Fg 3 | 4.67 | 4.00 | 7.0 | 0.03 | 0.09 | 10 | 0 | 11 | | |
| 353.3+06.3 | M 2-6 | 4.74 | 3.20 | 8.4 | 0.06 | 0.11 | 22 | 34 | 13 | 8.73 | |
| 353.5-04.9 | H 1-36 | 5.08 | 3.80 | 7.0 | 0.03 | 0.08 | 19 | 29 | 17 | | |
| 355.1-02.9 | H 1-31 | 5.04 | 3.70 | 12. | 0.04 | 0.11 | 21 | 31 | 19 | 8.77 | |
| 355.1-06.9 | M 3-21 | 4.95 | 3.20 | 5.0 | 0.06 | 0.11 | 18 | 28 | 16 | | |
| 355.4-02.4 | M 3-14 | 4.90 | 3.80 | 6.0 | 0.08 | 0.35 | 23 | 22 | 23 | 8.79 | |
| 355.7-03.5 | H 1-35 | 4.65 | 4.00 | 8.0 | 0.04 | 0.14 | 10 | 0 | 11 | | |
| 356.2-04.4 | Cn 2-1 | 4.92 | 3.60 | 6.0 | 0.03 | 0.07 | 23 | 22 | 21 | 8.94 | |
| 356.9+04.5 | M 2-11 | 5.15 | 2.70 | 7.0 | 0.05 | 0.06 | 20 | 20 | 17 | | |
| 357.2+07.4 | M 4-3 | 4.80 | 3.62 | 8.0 | 0.05 | 0.14 | 18 | 25 | 14 | 8.68 | |
| 358.2+03.6 | M 3-10 | 4.97 | 2.80 | 5.0 | 0.04 | 0.04 | 25 | 30 | 22 | 8.84 | |
| 358.5-04.2 | H 1-46 | 4.60 | 4.00 | 7.0 | 0.02 | 0.05 | 5 | 0 | 7 | | |
| 358.7-05.2 | H 1-50 | 5.00 | 3.30 | 7.6 | 0.03 | 0.05 | 26 | 31 | 22 | 8.80 | |
| 359.3-00.9 | Hb 5 | 5.08 | 3.50 | 1.3 | 0.02 | 0.03 | 25 | 39 | 21 | | |
| 359.7-02.6 | H 1-40 | 4.85 | 3.60 | 7.8 | 0.02 | 0.04 | 21 | 22 | 19 | 8.45 | |
| 359.8-07.2 | M 2-32 | 4.90 | 3.60 | 7.0 | 0.06 | 0.19 | 29 | 34 | 25 | | |
| 359.9-04.5 | M 2-27 | 4.70 | 3.60 | 5.5 | 0.03 | 0.06 | 26 | 41 | 17 | 8.83 | |

inner nebular region. The models correct for this effect, defining $\langle v_{\rm exp}\rangle$ as a global parameter of the nebula. We calculated the mean values which are respectively: $\langle v_{\rm exp}\rangle = 21\,{\rm km\,s^{-1}}$, $v_{\rm HWHM} = 18{\rm km\,s^{-1}}$. The mean ionized mass is $0.16\,{\rm M}_\odot$.

### *4.2. Comparison with other expansion velocity data*

The largest data set for expansion velocities of Galactic PNe is the catalog of Weinberger (1989) which is included in the ESO-Strasbourg Catalog of Galactic PNe (CGPN: Acker et al. 1992). The available data include measurements both in the [O III] and [N II] lines, although for many objects only [O III] has been measured. Sabbadin (1984) presented a previous catalogue of expansion velocities of 165 PNe, mostly based on [O III] line profiles. Dopita et al. (1985 and 1988) present [O III] expansion velocities for PNe in the SMC and the LMC respectively. Because they are relatively faint, few measurements of Bulge PN have so far been made.

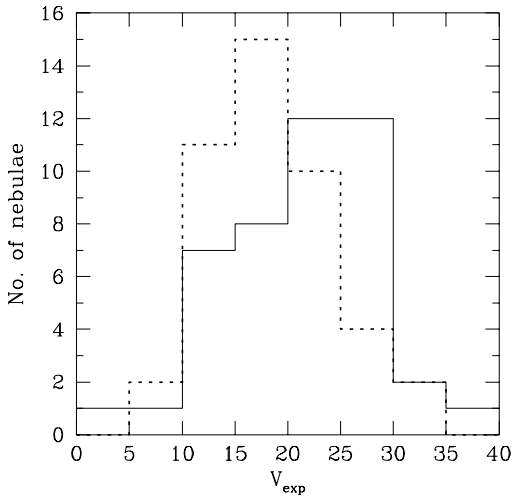


**Fig. 6.** Histogram of expansion velocities. The continuous line corresponds to the $\langle v_{\rm exp} \rangle$ values of models, the dashed line corresponds to $v_{\rm HWHM}$ estimated from the line profile.

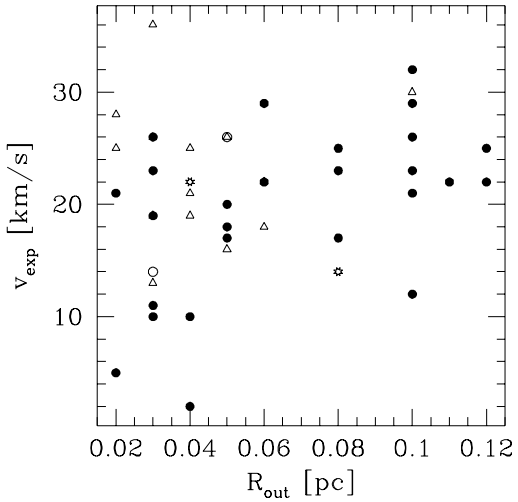


**Fig. 7.** Expansion velocity versus outer radius. Filled circles: Bulge PNe; triangles: Disk PNe; Stars: Halo PNe; open circles: Sgr PNe.

**Table 3.** The expansion velocities estimated from half width at half maximum of the asymmetric [O III] line profiles

| PN G | name | $v_{\rm HWHM}$ [km s$^{-1}$] | remarks |
|---|---|---|---|
| 000.7-02.7 | M 2-21 | 37 | |
| 348.0-13.8 | IC 4699 | 29 | |
| 351.6-06.2 | H 1-37 | 16 | bipolar outflow |
| 358.3-21.6 | IC 1297 | 22 | [WC4] |
| 359.1-01.7 | M 1-29 | 23 | |

The expansion velocities in Sabbadin's catalogue were derived in a variety of ways, but mostly from line splitting. Weinberger also primarily uses line splitting, but lists more values for [N II] and H$\alpha$. Note that both catalogues present twice the expansion velocity. Observations were typically taken at a resolution of 10–20 km s$^{-1}$.

Because of the way of measuring the expansion velocity, these values cannot be readily be compared with ours. For [O III], the published values may have been underestimated (see Fig. 1). Some measured velocities were reduced to correct for the presence of velocity gradients (e.g. Bianchi 1992). The MCs values of Dopita et al. are based on half width at ten per cent of the maximum. Table 1 shows that such a definition overestimates the velocity, but in the case of a velocity gradient their velocity is biased towards the outermost velocity and would be much larger than our mass-weighted average velocity.

### *4.3. Radius versus expansion velocity*

Several papers have noticed a correlation between nebular radius and expansion velocity (e.g. Robinson et al. 1982, Sabbadin 1984, Bianchi 1992). These relations were based on [O III] expansion velocities, and used statistical distances. Chu et al. (1984) show that when instead of the [O III] line the [O II] is used, only a very weak correlation remains for the most compact nebulae. Compact nebulae tend to have cooler central stars, and their [O III] emission arises from near the inner radius. The internal velocity gradient causes these velocities to be artificially low.

Fig. 7 shows our data: the only relation which seems to exist is that at small radii, a number of Bulge PN have very low expansion velocities, which are absent at larger nebulae. However, other Bulge PNe at the same radii do show large velocities. Among the disk PNe, there are no objects at small radii and low velocities. The sample is too small to judge whether this difference between the populations is real.

For very large, nearby PNe, the expansion velocities are known to decrease with radius. However, this strongly depends on the height above the Galactic plane: Hippelein & Weinberger (1990) show that for PNe larger than 0.25 pc radius, the mean expansion velocity is 10 km s$^{-1}$ in the plane but 35 km s$^{-1}$ at $z = 1$ kpc. The decrease in expansion velocity therefore seems related to deceleration by the ISM. In the Bulge, where the ISM is relatively unimportant, one would expect little deceleration. Interestingly, no Bulge PN larger than 0.2 pc is known. This may be related to a lack of ISM, so that the ionized mass does not increase beyond of the order of 0.2 M$_\odot$. This would cause large PNe to quickly diminish in brightness.

### *4.4. Evidence for acceleration*

The expansion velocity field of a planetary nebula arises from the original AGB wind, accelerated by interacting winds and ionization. The kinetic energy in the expansion can thus be seen as the original kinetic energy of the AGB wind, plus the amount deposited by the fast wind from the PN core. The original AGB wind has a near-constant velocity with radius; the gradient in the PN velocity field is caused by the interacting winds and the ionization (Schönberner & Steffen 1999, 2000).

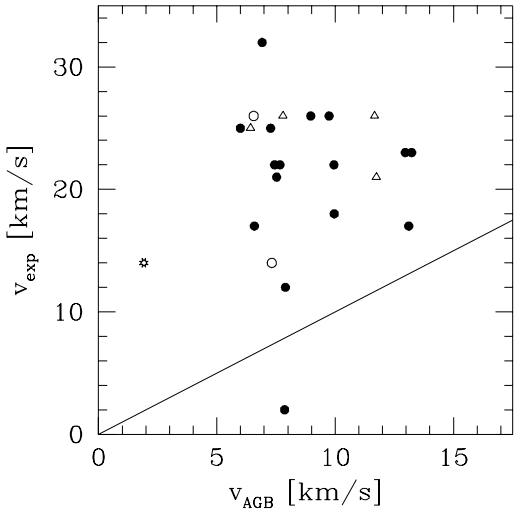


**Fig. 8.** PN expansion velocity versus the original AGB expansion velocity, calculated as described in the text. Symbols as in Fig. 7.

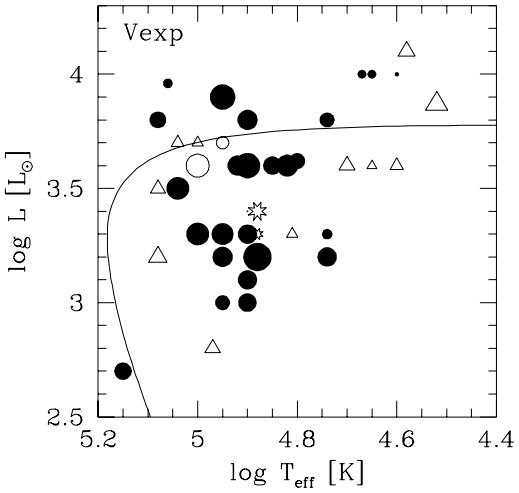


**Fig. 9.** HR diagram for the PNe. Symbols as in Fig. 7. Size of the symbol is proportional to the expansion velocity.

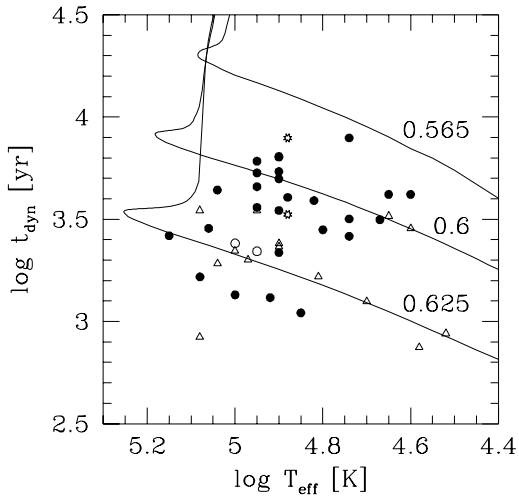


**Fig. 10.** The corrected dynamical age of the PNe, versus effective temperature of the star. The tracks correspond to theoretical models with core masses of 0.565, 0.6 and 0.625 $M_\odot$. Symbols as in Fig. 7.

The original AGB outflow velocity $v_{\rm AGB}$ can be estimated if the luminosity and metallicity of the star is known. Habing et al. (1994) show that $v_{\rm AGB} \propto L_*^{0.33}\delta^{0.5}$ where $\delta$ is the dust-to-gas ratio. For mass-loss rates above $10^{-5}\ M_\odot yr^{-1}$ the velocities are almost independent of mass-loss rates. We have calculated $v_{\rm AGB}$ for the PNe with known metallicity (using the O/H in Table 2). We assumed that a star with solar metallicity (O/H=8.93) has an AGB outflow velocity of 15 km s$^{-1}$. Fig. 8 plots $\langle v_{\rm exp}\rangle$ against $v_{\rm AGB}$. All but one object are expanding faster than their original AGB wind, typically by a factor of 2. This is direct evidence for the acceleration processes even for the most compact objects (in contrast to the result of Gussie & Taylor 1994). There is little evidence that $\langle v_{\rm exp}\rangle$ depends on the original AGB velocity: most of the memory of this wind is lost in the ionized region of a PN. We note that the single object with a very low abundance in our sample also has a low $v_{\rm exp}$ which could be a residual effect of its very low predicted $v_{\rm AGB}$. However, confirmation would require a much larger sample.

## 5. Nebulae and their central stars

### *5.1. HR diagram*

Fig. 9 shows the positions of the observed PNe in the HR diagram, for the four populations. The luminosities are not well determined: they will be underestimated if the PN is optically thin in some directions, i.e. if it leaks. Overplotted is an evolutionary track of Blöcker (1995), for a core mass of 0.6 $M_\odot$ (Gorny et al. 1997). Only one object is located on the cooling track: all other objects are consistent with the horizontal, hydrogen-burning part of the post-AGB track, allowing for uncertainty in the luminosities. The size of the symbols is proportional to $\langle v_{\rm exp}\rangle$. Among the Bulge PNe there are a few young objects (with cool central stars) with low expansion velocities, but otherwise little correlation is seen.

The luminosities are insufficiently accurate to draw quantitative conclusions for the central stars of our sample.

### *5.2. Dynamical ages*

The dynamical age of a PN is normally defined as the radius divided by the expansion velocity. This ignores the effects of the velocity gradient, as well as the acceleration over time. Dopita et al. (1996) calculate correction factors, based on semi-empirical relations, to convert dynamical ages to actual ages: they are typically around 1.5.

We calculate the dynamical age based on the average of $\langle v_{\rm exp}\rangle$ and $v_{\rm AGB}$, as a first-order estimate of the effect of acceleration. $v_{\rm AGB}$ is calculated as before, but where the metallicity is not known we took $v_{\rm AGB} = 0.5 \times v_{\rm exp}$. To account for the velocity gradient, we used a radius of 0.8 times the outer radius (since our velocity is based on a mass-weighted average). The resulting dynamical ages are plotted against $T_{\rm eff}$ of the star (which is well determined from our models) in Fig. 10.

The lines show predicted ages versus temperature for three post-AGB models with core masses of 0.565, 0.6 and 0.625 $M_\odot$ (adopted from Schönberner 1983; Gorny et al. 1997 and Blöcker 1995 respectively). Even over this small range of stellar masses, the evolutionary time scales for the increase in stellar temperature varies by a factor of 10. The models include the effect of post-AGB mass loss. For stars which leave the AGB as helium burners, stellar evolution slows down by about a factor of 3. A few objects could be explained as helium burners, but most Bulge PNe are well fitted by the models.

The uncertainty in the dynamical ages come from two factors. First, the use of [O III] lines only which do not allow us to determine the expected faster acceleration in the outer nebular regions. To first order this is corrected for because we use a radius which is smaller than the outer radius, and corresponds to the way the mass-weighted expansion velocity is defined. Hydrodynamical calculations which would allow a more accurate treatment are not presently available. Second, the direct averaging between the PN expansion velocity and the AGB velocity is ad-hoc: the associated uncertainty can reach 50% which would result in an uncertainty of 0.2 in $\log t_{\rm dyn}$.

### *5.3. Masses of nebular cores*

The derived dynamical ages plotted in Fig. 10 show that, in this sample, average core masses are in the range 0.60–0.625 $M_\odot$. PNe associated with the disk appear to have slightly higher core masses than Bulge PNe. Of the two halo PNe, one (M2-29) has a low core mass of around 0.58 $M_\odot$. The two PNe in Sgr have somewhat higher central-star masses of approximately 0.62 $M_\odot$. The uncertainties discussed introduce an systematic error in the derived masses of about 0.02 $M_\odot$. The *relative* uncertainties are much smaller since the uncertainties are derived from the way the ages are calculated.

The core masses agree well with Gorny et al. (1997) and Stasinska et al. (1997) for Galactic disk PNe: For an assumed nebular mass of 0.1 $M_\odot$, their median core mass is 0.60 $M_\odot$. Higher assumed nebular masses would shift the mass down to 0.58 $M_\odot$ for 0.4-$M_\odot$ nebulae. As noted by Stasinska et al., the most likely range for nebular masses is 0.1–0.15 $M_\odot$. Best agreement is indeed obtained for this range.

Sofar we have only used the relative location of the PNe with respect to the theoretical tracks. To obtain more precise values for the stellar mass, we use the fact that the three tracks are almost parallel for $5.0 > \log T > 4.6$. In this range, the location of the tracks can be fitted with the following relation: $M_{\rm c} = 0.6133 + 0.07\Delta - 0.04(\Delta + 0.19)^2$ where $\Delta = 0.72 \log T_{\rm eff} - \log t_{\rm dyn}$. The resulting masses are shown in Fig. 11, as a histogram. The Bulge and disk objects are shown by the drawn and dashed lines respectively. Fig. 11 indicates a tendency towards higher core masses for disk PNe. This can qualitatively be understood, since disk PNe will on average come from younger stars: higher initial mass would be expected to give higher final mass.

Fig. 11 shows that four Bulge PNe in our sample have core masses around $M_{\rm c} = 0.63\,{\rm M}_\odot$. The sample includes the most metal-rich Bulge PN. The radial velocities confirm that these objects really are located in the Bulge. These stars may have belonged to the inner disk population, having recently diffused into the Bulge through interaction with a Bar (Norman et al. 1996). The results of Ortolani et al. (1995) are based on clusters in the Bulge, and a younger diffused stellar population in the Bulge would not necessarily be contradicted by the old globular clusters.

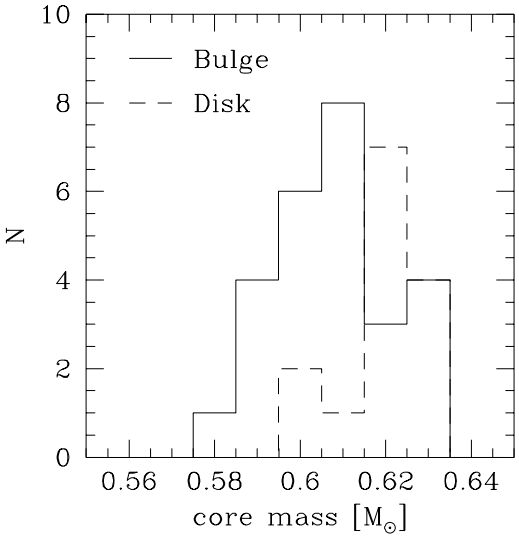


**Fig. 11.** Histogram of estimated core masses for Bulge and disk planetary nebulae. Systematic uncertainty on the masses is 0.02 $M_\odot$.

We finally note that the two PNe in Sgr also have somewhat higher core masses of approximately 0.62 $M_\odot$. This is consistent with the star formation history of Sgr: the progenitor stars are expected to be around 5 Gyr old (Dudziak et al. 2000). The halo PN with very low metallicity, on the other hand, has a lower core mass than the Bulge PNe. This could indicate that its progenitor star formed earlier than those of the Bulge PNe in our sample.

The core masses are strictly related to theoretical, hydrogen-burning evolutionary tracks. There is some uncertainty in these models regarding post-AGB mass loss. This would mainly affect the early part of the post-AGB evolution: at the temperature range in our sample, stellar mass loss is observed to be much less than the nuclear burning rate. The effect of model uncertainties are beyond the scope of the present paper. However, we note that Dudziak et al. (2000) determined accurate luminosities for the Sgr PNe, which are consistent with core masses around $0.61\,{\rm M}_\odot$. Thus, the combined errors from models and our determination may be within $0.02\,{\rm M}_\odot$.

### *5.4. Comparison with white dwarf masses*

The core mass of the central star of a PNe is (within $10^{-3}\,{\rm M}_\odot$) the same as the mass of the resulting white dwarf. The Bulge PNe therefore measure the initial-final mass relation for low-mass stars. The Bulge population is among the oldest in the Galaxy (Ortolani et al. 1995) with a well-determined turn-off mass: $M_{\rm i} \approx 1\,{\rm M}_\odot$ and $t = 10^{10}\,{\rm yr}$. The metallicity is also

known to be not far from solar. For these numbers, the initial-final mass relation proposed by Weidemann (1987) predicts final masses around $M_{\rm f} = 0.55\,{\rm M}_{\odot}$. Our results indicate that this is too low by about 10 per cent. The good agreement with Stasinska et al. confirms our higher value.

We can also compare the core mass distribution to the mass distribution of white dwarfs in the solar neighbourhood. Bragaglia et al. (1995) find that the local white dwarf mass distribution shows a peak at $M_{\rm WD} = 0.55\,{\rm M}_{\odot}$, with tails towards both higher and lower masses. Napiwotzki et al. (1999) find a peak at higher masses, at $M_{\rm WD} = 0.59\,{\rm M}_{\odot}$, which is within the uncertainties of the present determination for the Bulge. It should be noted that the determinations should not necessarily agree: Stars in the Bulge could evolve to somewhat higher core masses than stars in the solar neighbourhood, if the AGB superwind is less efficient at lower metallicity. Also, PNe trace the *present* main-sequence turn-off stars while the white dwarf population has accumulated over time. The effect is complicated by cooling which renders the white dwarf eventually undetectable, and is dependent on the mass (Hansen 1999). The masses of local white dwarfs may also have been underestimated. This is discussed in Bragaglia et al. (1995) who find that if the hydrogen layer in the white dwarfs is much thicker than assumed, the spectroscopic masses should be increased by $\sim 0.04\,{\rm M}_{\odot}$.

In view of these uncertainties, the agreement especially with the result of Napiwotzki is satisfactory. The discrepancy with the initial-final mass relations is however much larger than the present uncertainties, and must be considered significant.

## 6. Conclusions

We have presented the first study of expansion velocities and dynamical ages of Bulge and halo PNe, using expansion velocity profiles. A constant expansion velocity is found not to be a good approximation, but a linear velocity field fits the observed [O III] 5007 Å line shapes relatively well. Such a velocity field is in qualitative agreement with predictions from hydrodynamical models, allowing for the fact that the [O III] traces the inner regions only.

Expansion velocities determined from line splitting are shown to underestimate the true velocities. The FWHM gives a better approximation. We note that expansion velocities measured by different methods or from different lines cannot be easily compared.

A relation between expansion velocity and outer radius, as claimed by several previous papers, is not confirmed by our data. The only weak correlation is that Bulge PN with a very small radius ($< 0.05\,{\rm pc}$) may show low velocities. No clear correlation is seen for expansion velocities against other stellar parameters, nor are the halo and Sgr PNe systematically different.

Dynamical ages are calculated using an approximation for the effects of acceleration and non-uniform velocities. We estimate the original AGB outflow velocities for our stars, and show that the nebulae have undergone acceleration by about a factor of 2. The inner regions of the nebulae show little memory of the original velocities, with the possible exception of a single object with very low metallicity.

Finally we derived core masses of PNe from our sample. This was accomplished by comparing our dynamical ages with the timescales of theoretical evolutionary tracks of Schönberner (1983) and Blöcker (1995). The average core masses are in the range of 0.60–0.625 $\rm M_{\odot}$, with slightly higher values for the disk objects than for those from Galactic Bulge. The resulting masses show good agreement with Gorny et al. (1997) and Stasinska et al. (1997) who apply a different method but use the same evolutionary tracks.

*Acknowledgements.* This project was partially supported by the British-Polish Joint Research Collaboration Programme. K.Gesicki acknowledges partial support from Polish KBN grant No. 2.P03D.002.13. We thank Agnes Acker for providing the [NII] data in Fig. 2. Jeremy Walsh was involved in the observations; he is also thanked for careful reading of the manuscript.

## References

Acker A., Ochsenbein F., Stenholm B., et al., 1992, Strasbourg – ESO Catalogue of Galactic Planetary Nebulae. ESO, Garching (CGPN)
Aller L., Keyes C., 1987, ApJS 65, 405
Bianchi L., 1992, A&A 260, 314
Blöcker T., 1995, A&A 299, 755
Bragaglia A., Renzini A., Bergeron P., 1995, ApJ 443, 734
Chu Y.-H., Kwitter K.B., Kaler J.B., Jacoby G.H., 1984, PASP 96, 598
Costa R., de Freitas Pacheco J.A., de Franca Jr J.A., 1996, A&A 313, 924
Cuisinier F., Maciel W.J., Köppen J., Acker A., Stenholm B., 2000, A&A 353, 543
Dopita M.A., Ford H.C., Lawrence C.J., Webster B.L., 1985, ApJ 296, 390
Dopita M.A., Meatheringham S.J., Webster B.L., Ford H.C., 1988, ApJ 327, 639
Dopita M.A., Vassiliadis E., Meatheringham S.J., et al., 1996, ApJ 460, 320
Dudziak G., Pequignot D., Zijlstra A.A., Walsh J.R., 2000, A&A, submitted
Gesicki, K., Acker, A., 1996, Ap&SS 238, 101
Gesicki K., Acker A., Szczerba R., 1996, A&A 309, 907 (Paper I)
Gesicki K., Zijlstra A.A., Acker A., Szczerba R., 1998, A&A 329, 265 (Paper II)
Gorny S.K., Stasinska G., Tylenda R., 1997, A&A 318, 256
Gussie G.T., Taylor A.R., 1994, PASP 106, 500
Habing H.J., Tignon J., Tielens A.G.G.M., 1994, A&A 286, 523
Hansen B.M.S., 1999, ApJ, 520, 680
Hippelein H., Weinberger R., 1990, A&A 232, 129
Marten H., Schönberner D., 1991, A&A 248, 590
Minniti D., 1996, ApJ 459, 579
Napiwotzki R., Green P.J., Saffer R.A., 1999, ApJ 517, 399
Norman, C.A., Sellwood J.A.. Hasan H., 1996, ApJ 462, 114
Ortolani S., Renzini A., Gilmozzi R., et al., 1995, Nat 377, 701
Pottasch S.R., 1984, Planetary Nebulae, Reidel, Dordrecht
Ratag M.A., Pottasch S.R., Dennefeld M., Menzies J.W., 1997, A&AS 126, 297
Robinson G.J., Reay N.K., Atherton P.D., 1982, MNRAS 199, 649
Sabbadin F., 1984, A&AS 58, 273
Schönberner D., 1983, ApJ 272, 708

Schönberner D., Steffen M., 1999, in: Guenther E.W., Stecklum B., Klose S. (eds.), Optical and infrared spectroscopy of circumstellar matter ASP Conf. Ser., Vol. 188, p. 281
Schönberner D., Steffen M., 2000, in: Kastner J.H., Soker N., Rappaport S. (eds.), Assymetrical Planetary Nebulae II: From Origins to Microstructures, ASP Conf. Ser., vol. 199
Stasinska G., Gorny S.K., Tylenda R., 1997, A&A 327, 736
Van de Steene G.C., Zijlstra A.A., 1994, A&AS 108, 485
Webster B.L., 1988, MNRAS 230, 377
Weidemann V., 1987, A&A 188, 74
Weinberger R., 1989, A&AS 78, 301
Wilson O.C., 1950, ApJ 111, 279
Zijlstra A.A., Walsh J.R., 1996, A&A 312, L21
Zijlstra, A.A., Pottasch, S.R., Bignell, C., 1989, A&AS 79, 329
Zijlstra A.A., Acker A., Walsh J.R., 1997, A&AS 125, 289